Vol 461|1 October 2009|doi:10.1038/nature08395

LETTERS

Remote triggering of fault-strength changes on the San Andreas fault at Parkfield

Taka'aki Taira[1], Paul G. Silver[1]‡, Fenglin Niu[2] & Robert M. Nadeau[3]

Fault strength is a fundamental property of seismogenic zones, and its temporal changes can increase or decrease the likelihood of failure and the ultimate triggering of seismic events. Although changes in fault strength have been suggested to explain various phenomena, such as the remote triggering of seismicity[1], there has been no means of actually monitoring this important property *in situ*. Here we argue that ~20 years of observation (1987–2008) of the Parkfield area at the San Andreas fault have revealed a means of monitoring fault strength. We have identified two occasions where long-term changes in fault strength have been most probably induced remotely by large seismic events, namely the 2004 magnitude (M) 9.1 Sumatra–Andaman earthquake and the earlier 1992 $M = 7.3$ Landers earthquake. In both cases, the change possessed two manifestations: temporal variations in the properties of seismic scatterers—probably reflecting the stress-induced migration of fluids—and systematic temporal variations in the characteristics of repeating-earthquake sequences that are most consistent with changes in fault strength. In the case of the 1992 Landers earthquake, a period of reduced strength probably triggered the 1993 Parkfield aseismic transient[2–5] as well as the accompanying cluster of four $M > 4$ earthquakes at Parkfield. The fault-strength changes produced by the distant 2004 Sumatra–Andaman earthquake are especially important, as they suggest that the very largest earthquakes may have a global influence on the strength of the Earth's fault systems. As such a perturbation would bring many fault zones closer to failure, it should lead to temporal clustering of global seismicity. This hypothesis seems to be supported by the unusually high number of $M \geq 8$ earthquakes occurring in the few years following the 2004 Sumatra–Andaman earthquake.

The time-varying properties of seismic scatterers have recently been used to probe stress-induced changes in the San Andreas fault zone near Parkfield in central California[4]. This temporal variability is most clearly observable through the use of repeating earthquakes that minimize variations in the source location and mechanism that could be mapped as apparent changes in the medium[4,6,7]. As a measure of temporal scatterer behaviour from one earthquake to the next, we made use of decorrelation index $D(t)$ derived from the cross-correlation of two seismograms (Supplementary Fig. 1 and Methods). Using particularly tightly clustered repeating microearthquakes[8,9] recorded by the High-Resolution Seismic Network (HRSN; Fig. 1), we have been able to track the behaviour of a group of time-dependent scatterers for a 22-year period (1987–2008); we will refer to this group of scatterers, first identified in ref. 4, as the target scatterer.

We find three excursions. The first excursion in $D(t)$ appears to have initiated between 10 September 1992 and 5 February 1993 (Supplementary Fig. 2). It reaches a peak in the mid 1990s and then gradually decays over the next decade (Fig. 2a). This variation closely tracks a well-documented transient in fault slip-rate along the San Andreas fault, as inferred from both geodetic measurements[2,3,5] and a change in seismic slip rate[9], $\dot{d} = M_0/T_r$, calculated from the recurrence interval, T_r, and seismic moment, M_0, of repeating earthquakes[9–11]. This excursion has been interpreted as reflecting stress-induced fluid migration associated with the 1993 Parkfield aseismic transient (ref. 4 and Supplementary Fig. 3).

The second excursion in target-scatterer properties is constrained to have initiated during the interval spanning the 28 September 2004

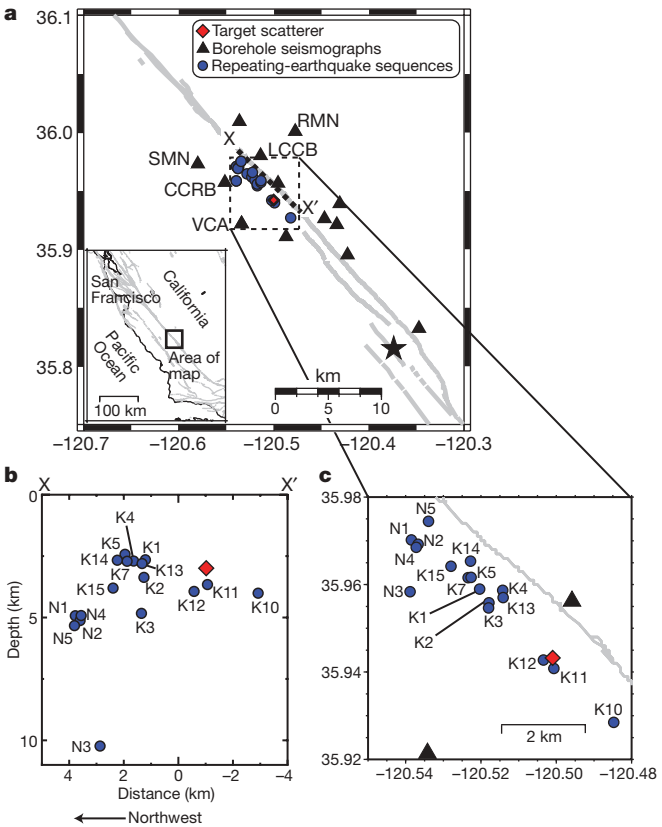

Figure 1 | Map of the Parkfield segment at the San Andreas fault. **a**, Locations of the target scatterer (red diamond), the HRSN borehole stations (triangles) and 17 repeating-earthquake sequences (circles) (ref. 8 and Methods). Labelled stations are those used in this study. The other stations either have a high noise level, are dominated by fault-zone guided waves, or do not respond to the scatterer defined by ref. 4. Star is the epicentre of the 2004 Parkfield earthquake. **b**, Vertical cross-section along X–X′ in **a**. **c**, Detailed map view.

[1]Department of Terrestrial Magnetism, Carnegie Institution of Washington, District of Columbia 20015, USA. [2]Department of Earth Science, Rice University, Houston, Texas 77005, USA. [3]Berkeley Seismological Laboratory, University of California, Berkeley, California 94720, USA.
‡Deceased.

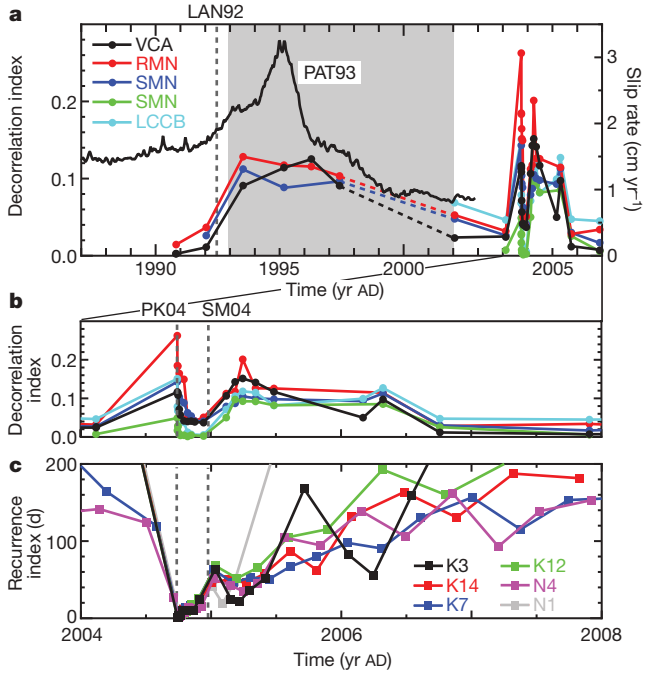

Figure 2 | Temporal changes in scatterer properties for a 22-year period. **a**, **b**, $D(t)$ reflecting target-scatter properties (Methods) for sequence K3 recorded by five stations during 1987–2008 (**a**) and 2004–08 (**b**). **c**, T_r for six sequences plotted at the midpoint between the origin times of the two events. Broken lines indicate HRSN was not functional (1998–2001). Solid line is geodetic inferred slip rate[5] that is concentrated in the section of the fault studied here (figure 5 in ref. 5). Vertical dashed-grey lines denote occurrence times of 1992 Landers (LAN92), 2004 Parkfield (PK04) and 2004 Sumatra–Andaman (SM04) earthquakes. PAT93 denotes the 1993 Parkfield aseismic transient (shaded area).

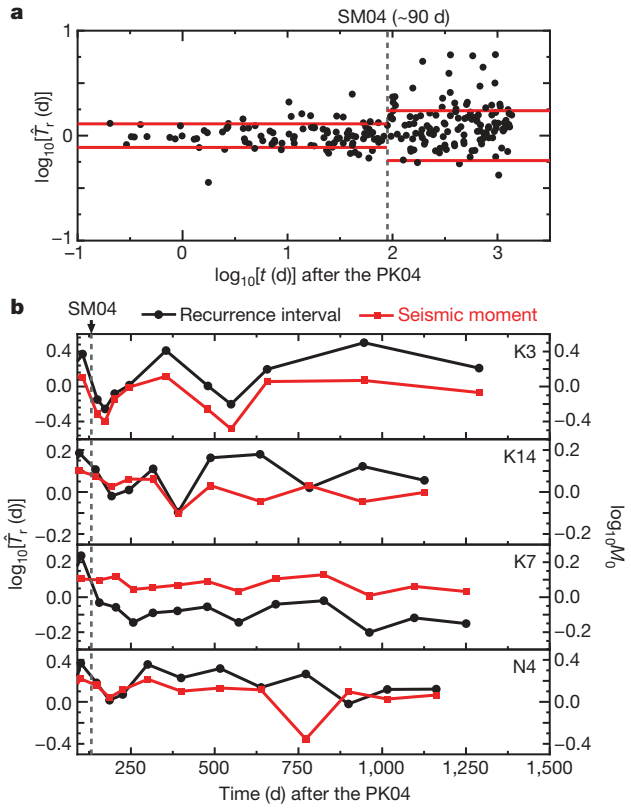

Figure 3 | Temporal variations in $\hat{T}_r$ following the 2004 Sumatra–Andaman earthquake. **a**, $\hat{T}_r$ for all available sequences. Red lines indicate standard deviations of $\hat{T}_r$. These variations are 0.11 and 0.24 for pre- and post-2004 Sumatra–Andaman earthquake periods, respectively. **b**, $\hat{T}_r$ (black circles) and M_0 (red squares) for four sequences. $\hat{T}_r$ and M_0 closely track each other, which suggests they reflect the time history of fault strength (see Supplementary Fig. 6). $\hat{T}_r$ is plotted at the midpoint between the origin times of the two events. M_0 of the second event in a pair is plotted at the same midpoint, and was normalized by its average value for the entire time period for each sequence.

$M_w = 6.0$ Parkfield earthquake[7] (from 24 days before to 2 hours after), and is thus consistent with an instantaneous coseismic change in $D(t)$ (Supplementary Fig. 4). The excursion then decays back to the pre-earthquake level after about 2–3 months (Fig. 2b). The observed structural changes are probably due to fluid redistribution around the fault resulting from a combination of both post-seismic stress relaxation[12] and direct fault-zone damage[13].

A third excursion in $D(t)$ occurred about three months after the 2004 Parkfield earthquake (Fig. 2b). The magnitude of change in $D(t)$ is comparable to that observed for the other two transients. The increase in $D(t)$ takes place over three months, after which time $D(t)$ decays slowly over a subsequent ~1 year period (Supplementary Fig. 5).

There are also changes in repeating-earthquake properties that accompany this third excursion in $D(t)$. Following the 2004 Parkfield earthquake, there is a characteristic increase in T_r, as is typically observed postseismically[14]. This trend, however, is interrupted roughly three months after the 2004 Parkfield earthquake (Fig. 2c). In 6 of the available 13 sequences, there is a systematic reduction in T_r that reaches a minimum about 6 months after the 2004 Parkfield earthquake. To explore this apparent disruption further, we removed the post-seismic effect produced by the 2004 Parkfield earthquake, assuming Omori's law, $T_r(t) = at^p$ (ref. 15 and Methods), and computed the residual recurrence interval, $\hat{T}_r(t) = T_r(t)/(at^p)$, where t is time after the earthquake, and a and p are constants to be estimated. Using all available sequences, we find that the logarithm of the residuals increases by roughly a factor of 2, beginning three months after the 2004 Parkfield earthquake (Fig. 3a). This increased variability suggests an additional perturbation to T_r and a temporal change in the mechanical properties of the fault.

An interesting feature of this variability is that there is a positive correlation between $\hat{T}_r$ and M_0 (Fig. 3b). Such a correlation is consistent with a slip-predictable model for earthquake occurrence[16], where the stress drop and T_r are both determined by the failure strength of the fault, for constant loading rate and constant minimum stress (Supplementary Fig. 6). Assuming rupture area is constant among members of a repeating-earthquake sequence[8], then fault slip will be proportional to M_0 which should in turn be proportional to stress drop.

The most dramatic correlation that we found is for sequence K3 (5 km depth; Fig. 3b). This sequence also has the least variability in event location, so that the assumption of constant fault area should be the most valid[8]. The correlation between $\hat{T}_r$ and M_0 suggests variations in fault strength over a factor of two, three months after the 2004 Parkfield earthquake. A reduction in $\hat{T}_r$ (and M_0) around 6 months after the 2004 Parkfield earthquake (Fig. 2c) indicates a temporary weakening of the fault (Fig. 3b).

We have localized the onset time of the third excursion in $D(t)$ using all of the repeating-earthquake sequences that displayed a change in $D(t)$ (Supplementary Fig. 7). We find that the excursion must have initiated between 21 December (sequence K2) and 26 December 2004 (sequence K5) (Supplementary Fig. 7b). The most dramatic tectonic event to occur within the 5-day time window is the 26 December 2004 $M_w = 9.1$ Sumatra–Andaman earthquake, whose origin time is 7 h before the end of the interval (Supplementary Fig. 7c). The timing strongly suggests that the dynamic stresses from this earthquake, estimated to be about 10 kPa (based on the amplitude of long period surface waves (>30 s) which are likely to have the strongest impact on fluid flow[17]), induced fluid flow that caused both a structural change in the fault zone region (that is, changes in $D(t)$) and, through variations

in pore pressure, consequent changes in the strength of the fault. It is now well documented that such dynamic stresses are capable of remotely triggering seismicity[18,19]. The present study suggests that these same dynamic stresses can actually produce long-term (~1 year for our study) changes in fault strength.

Given the behaviour of the third excursion, in particular the likely influence of a very large remote event, it is worthwhile revisiting the first excursion. Although initially interpreted as being produced by the 1993 Parkfield aseismic transient[4], similarities in the behaviour of $D(t)$ between the third and first excursions raise the possibility of remote triggering. Indeed, the largest observed dynamic stress change at Parkfield over the entire 22-year observing period is attributed to the 28 June 1992 $M_w = 7.3$ Landers earthquake, estimated to be 65 kPa, nearly an order of magnitude greater than for the 2004 Sumatra–Andaman earthquake. The Landers event triggered microseismicity throughout California and Nevada, both short-term (weeks)[18], as well as multiyear[20].

The excursion in $D(t)$ initiated a few months after the 1992 Landers earthquake. There were also changes in repeating-earthquake properties, namely a systematic reduction in M_0 (proportional to fault strength) from 6 of 17 available sequences following the 1992 Landers earthquake (Fig. 4). Moment reaches a minimum by the mid-1990s, during a time in which $D(t)$ and the geodetic slip rate both reach maxima[5]. All of these indicators subsequently returned to pre-1992 levels in advance of the 2004 Parkfield earthquake (Fig. 4). As with the third excursion, this overall behaviour suggests that the dynamic stresses of the 1992 Landers earthquake changed the structure and weakened the fault zone in the region of our study. In this interpretation, it is the 1992 Landers earthquake that triggered both the 1993 Parkfield aseismic transient as well as the accompanying cluster of four $M > 4$ earthquakes by weakening the fault[2,5].

Although there are many similarities between these two hypothesized episodes of remote triggering, there are also differences, which appear to be related to the occurrence of the 2004 Parkfield earthquake. First, the 1992 Landers earthquake apparently produced triggered slip on the San Andreas fault (both seismic and aseismic), whereas the 2004 Sumatra–Andaman earthquake did not. Second, for the 2004 Sumatra–Andaman earthquake, the onset of an observable change in $D(t)$ was essentially instantaneous, whereas it took months in the case of the 1992 Landers earthquake. Similarly, the corresponding changes

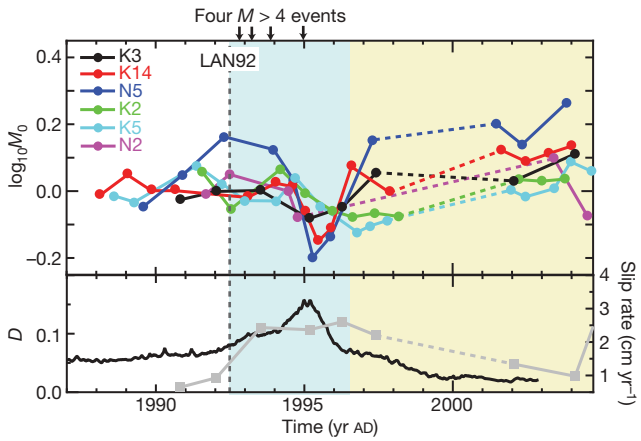

Figure 4 | Temporal changes in seismic moment for the post-Landers earthquake period. Top panel, reduction in M_0 is seen ~2–3 years after the 1992 Landers earthquake (LAN92, vertical dashed line), for 6 (of 17) sequences, suggesting temporary reduction in fault strength (see text). Arrows indicate four $M > 4$ earthquakes at Parkfield. M_0 for each sequence was normalized by average seismic moment from pre-1993 earthquakes. Bottom panel, geodetic slip rate[5] (solid line) and average $D(t)$ from sequence K3 (grey squares), using three stations (VCA, RMN and SMN). Blue (beige) field denotes inferred times of fault weakening (restrengthening). Broken lines indicate when HRSN was not functional.

in repeating-earthquake properties took a few months for the 2004 Sumatra–Andaman earthquake but a few years for the 1992 Landers earthquake. The third issue is sensitivity to dynamic stresses. There were three pre-Parkfield events in the 22-year observing period (1987–2008) that generated stresses roughly a factor of three greater than the 2004 Sumatra–Andaman earthquake (although a factor of 2 less than the 1992 Landers earthquake): the 3 November 2002 $M_w = 7.9$ Denali earthquake, the 16 October 1999 $M_w = 7.1$ Hector Mine earthquake, and the 22 December 2003 $M_w = 6.5$ San Simeon earthquake. They did not produce a detectable change in $D(t)$.

The 2004 Parkfield earthquake probably had two major effects on the fault zone. First, it damaged the fault zone by creating new fractures, as suggested by the dramatic post-seismic change in fault zone seismic properties[13]. Second, it relieved most of the stress stored in the fault zone. The timescale for fluid migration and resulting changes in fault strength should be a strong function of the fracture permeability of the medium. It is likely that Parkfield-earthquake-induced damage dramatically increased fracture permeability[21], thereby reducing the time constant for fluid migration after the earthquake. It also probably produced an increased sensitivity to dynamic stresses, thereby accounting for the positive response to Sumatra–Andaman dynamic stresses but not to the stronger 1999 Hector Mine, 2002 Denali and 2003 San Simeon dynamic stresses. Finally, the absence of accompanying slip for the 2004 Sumatra–Andaman earthquake can be explained by the low driving stress. Indeed, the hypothesized change in fault strength occurred after most of the Parkfield post-seismic deformation had already occurred.

Our inference that $D(t)$ is a proxy for fluid-induced changes in fault strength has several implications. First, it may be possible to continually monitor changes in fault strength, which is one of the most important parameters in assessing the seismogenic potential of a fault. Second, although clearly reflected in scatterer properties, such a fluid redistribution would be essentially undetectable by surface geodesy (in the absence of triggered slip), as the predicted signals are below the detection limits of currently available geodetic instruments (Supplementary Fig. 8 and Methods). The scatterers are thus measuring a fundamentally different physical property from that measured by geodesy. This would explain why the third excursion in $D(t)$ did not produce a detectable geodetic signal or a change in seismic slip rate, despite the change in scatterer properties and in fault strength inferred from repeating-earthquake systematics. Third, the effect on fault strength may be spatially heterogeneous, given that only about half of the repeating-earthquake sequences exhibited patterns consistent with fault weakening for both the Landers and Sumatra–Andaman earthquakes. This variability would be an expected consequence of fluid redistribution, which itself is likely to be spatially heterogeneous. Last, the long-range influence (~8,000 km) of the 2004 Sumatra–Andaman earthquake on this patch of the San Andreas fault suggests that many of the world's active faults were affected in the same way, thus bringing a significant fraction of them closer to failure. We speculate that such large events should produce a temporal clustering of global seismicity. This hypothesis appears to be supported by the unusually high number of $M \geq 8$ earthquakes occurring in the three years following the 2004 Sumatra–Andaman earthquake. No other large earthquake ($M \geq 8$) since 1900 was followed by as many for a comparable period.

METHODS SUMMARY

Cross-correlation analysis. We use two parameters derived from the cross-correlation of two seismograms, the lag time $\tau(t)$ and decorrelation index $D(t)$. We define $\tau(t)$ for a particular time window with centre (elapsed) time t as the lag that yields the maximum cross-correlation $C_{max}(t)$, and $D(t) = 1 - C_{max}(t)$ (ref. 4). We focus primarily on $D(t)$, because, unlike $\tau(t)$, it is insensitive to variations in the shallow near-station environment (Supplementary Fig. 1 and Methods).

Post-seismic effect on recurrence interval. We assume that T_r is governed by Omori's law, $T_r(t) = at^p$ (ref. 15), as a model of the expected increase in T_r due to a decay in fault-slip rate, where t is time after the earthquake and a and p are

constants to be estimated. Using data from the first three months of the post-Parkfield earthquake period and using all available sequences, we obtain a value of $p = 0.7$, comparable to what has been found in similar seismic studies[14], as well as to the geodetic data for this period[12].

Full Methods and any associated references are available in the online version of the paper at www.nature.com/nature.

Received 25 April; accepted 6 August 2009.

1. Hill, D. P. & Prejean, S. G. in *Treatise on Geophysics* (ed. Schubert, G.) Vol. 4 (ed. Kanamori, H.) 257–292 (Elsevier Science, 2007).
2. Langbein, J., Gwyther, R. L., Hart, R. H. G. & Gladwin, M. T. Slip-rate increase at Parkfield in 1993 detected by high-precision EDM and borehole tensor strainmeters. *Geophys. Res. Lett.* **26,** 2529–2532 (1999).
3. Gao, S., Silver, P. G. & Linde, A. T. Analysis of deformation data at Parkfield, California: detection of a long-term strain transient. *J. Geophys. Res.* **105** (B2), 2955–2967 (2000).
4. Niu, F., Silver, P. G., Nadeau, R. M. & McEvilly, T. V. Migration of seismic scatterers associated with the 1993 Parkfield aseismic transient event. *Nature* **426,** 544–548 (2003).
5. Murray, J. R. & Segall, P. Spatiotemporal evolution of a transient slip event on the San Andreas fault near Parkfield, California. *J. Geophys. Res.* **110,** B09407, doi:10.1029/2005JB003651 (2005).
6. Baisch, S. & Bokelmann, G. H. R. Seismic waveform attributes before and after the Loma Prieta earthquake: scattering change near the earthquake and temporal recovery. *J. Geophys. Res.* **106** (B8), 16323–16338 (2001).
7. Taira, T., Silver, P. G., Niu, F. & Nadeau, R. M. Detecting seismogenic stress evolution and constraining fault zone rheology in the San Andreas Fault following the 2004 Parkfield earthquake. *J. Geophys. Res.* **113,** B03303, doi:10.1029/2007JB005151 (2008).
8. Nadeau, R. M. & Johnson, L. R. Seismological studies at Parkfield VI: moment release rates and estimates of source parameters for small repeating earthquakes. *Bull. Seismol. Soc. Am.* **88,** 790–814 (1998).
9. Nadeau, R. M. & McEvilly, T. V. Fault slip rates at depth from recurrence intervals of repeating microearthquakes. *Science* **285,** 718–721 (1999).
10. Nadeau, R. M. & McEvilly, T. V. Periodic pulsing of characteristic microearthquakes on the San Andreas Fault. *Science* **303,** 220–222 (2004).
11. Bürgmann, R. *et al.* Earthquake potential along the Northern Hayward Fault, California. *Science* **289,** 1178–1182 (2000).
12. Langbein, J., Murray, J. R. & Snyder, H. A. Coseismic and initial postseismic deformation from the 2004 Parkfield, California, earthquake, observed by Global Positioning System, electronic distance meter, creepmeters, and borehole strainmeters. *Bull. Seismol. Soc. Am.* **96,** S304–S320 (2006).
13. Li, Y.-G., Chen, P., Cochran, E. S., Vidale, J. E. & Burdette, T. Seismic evidence for rock damage and healing on the San Andreas Fault associated with the 2004 M 6.0 Parkfield earthquake. *Bull. Seismol. Soc. Am.* **96,** S349–S363 (2006).
14. Peng, Z., Vidale, J. E., Marone, C. & Rubin, A. Systematic variations in recurrence interval and moment of repeating aftershocks. *Geophys. Res. Lett.* **32,** L15301, doi:10.1029/2005GL022626 (2005).
15. Schaff, D. P., Beroza, G. C. & Shaw, B. E. Postseismic response of repeating aftershocks. *Geophys. Res. Lett.* **25,** 4549–4552 (1998).
16. Shimazaki, K. & Nakata, T. Time-predictable recurrence model for large earthquakes. *Geophys. Res. Lett.* **7,** 279–282 (1980).
17. Brodsky, E. E. & Prejean, S. G. New constraints on mechanisms of remotely triggered seismicity at Long Valley Caldera. *J. Geophys. Res.* **110,** B04302, doi:10.1029/2004JB003211 (2005).
18. Hill, D. P. *et al.* Seismicity remotely triggered by the magnitude 7.3 Landers, California, earthquake. *Science* **260,** 1617–1623 (1993).
19. West, M., Sánchez, J. J. & McNutt, S. R. Periodically triggered seismicity at Mount Wrangell, Alaska, after the Sumatra earthquake. *Science* **308,** 1144–1146 (2005).
20. Gao, S. S., Silver, P. G., Linde, A. T. & Sacks, I. S. Annual modulation of triggered seismicity following the 1992 Landers earthquake in California. *Nature* **406,** 500–504 (2000).
21. Elkhoury, J. E., Brodsky, E. E. & Agnew, D. C. Seismic waves increase permeability. *Nature* **441,** 1135–1138 (2006).

Supplementary Information is linked to the online version of the paper at www.nature.com/nature.

Acknowledgements This work was supported by the National Science Foundation EAR-0337308, EAR-0408947, EAR-0409024, EAR-0453638, EAR-0537641, EAR-0544730 and DTM-2025-01, and by the Department of Terrestrial Magnetism, Carnegie Institution of Washington. The Parkfield High-Resolution Seismic Network is operated by University of California, Berkeley Seismological Laboratory with financial support from the US Geological Survey (USGS) through National Earthquake Hazards Reduction Program award 07HQAG0014. Seismic and geodetic data are archived at the Northern California Earthquake Data Center and USGS, respectively. We thank J. Murray-Moraleda for providing the slip rate data, and E. A. Roeloffs and A. T. Linde for discussions. This is Berkeley Seismological Laboratory contribution 09-14.

Author Contributions T.T., with P.G.S. and F.N, analysed data; R.M.N. identified and maintained the repeating earthquake catalogue; P.G.S. and T.T. wrote the manuscript with contributions from all authors.

Author Information Reprints and permissions information is available at www.nature.com/reprints. Correspondence and requests for materials should be addressed to T.T. (taira@dtm.ciw.edu).

METHODS

Data set. The 17 repeating-earthquake sequences we have examined span a depth range of ~10 km and along-fault distance of ~8 km. Sequences K4, K10, K13 and K15 have been updated to 1998.

Decorrelation index and lag times from cross-correlation analysis. $\tau(t)$ is defined as the mean travel time perturbation of the lag times, τ_i, associated with the individual scattered phases in the time window, while $D(t)$ can be defined as $\omega^2 s_\tau^2/2$ where s_τ and ω are the standard deviation of τ_i and the characteristic frequency of the scattered phases, respectively[22]. Thus $\tau(t)$ and $D^{1/2}(t)$ are proportional to the mean and standard deviation of a weighted distribution of lag times, respectively. A constant velocity reduction in the background medium should yield a linear trend in $\tau(t)$ and $D(t) = 0$, given a short time window for calculating $\tau(t)$ and $D(t)$.

On the other hand, a previous numerical experiment[4] illustrates that isolated spikes in $\tau(t)$ and $D(t)$ can be explained by local changes in the location of a scatterer or by a velocity reduction around the scatterer. Our interest is in detecting discrete scatterers that permit the imaging of fault-zone properties at seismogenic depth, rather than changes in the background medium. We have therefore focused on detection of isolated spikes in $D(t)$ rather than $\tau(t)$ because the latter potentially contains this shallow contribution.

Measurement of decorrelation index. To measure $D(t)$, the chosen reference events for stations VCA, RMN and SMN were taken to be pre-1993, while those for stations CCRB and LCCB occurred ~50 days after the 2004 Parkfield earthquake. Elapsed times used for measuring $D(t)$ for stations VCA, RMN and SMN were the same as those for the previous study[4]. For stations CCRB and LCCB (unavailable in previous study), the first clear isolated peak in $D(t)$ in S-coda was chosen. A 0.5-s time window was used for calculating $D(t)$. As a way of assessing the data quality, we computed median $D(t)$ in a 1-s time window after the direct P wave. This gives us a measure of $D(t)$ in a part of the seismogram where we do not expect a contribution from the medium (ref. 4). On this basis we ranked the stations, averaged over all sequences, and found the stations VCA, CCRB and LCCB to be our best stations. We also used the same procedure to obtain a noise level for $D(t)$ for each sequence that may then be used to define a level of significance (for example, Supplementary Fig. 7b). Finally, we only use data where the median $D(t)$ (in a 2-s time window after the direct P wave) is less than 0.1.

Predicted geodetic response for a redistribution of fluid. Assume that we have a vertical fluid-filled fracture at 5 km depth with dimension one square kilometre in size and 10 mm in width, and that fluid migrates 500 m laterally (that is, 500 m of the fracture closes at one end and opens at the other end). The resulting deformation signal can be expressed as the sum of two sources, both 1 km by 500 m in dimension, opposite in sign, and separated by one kilometre. Using an elastic half-space model[23] to calculate the surface deformation, we find that the resulting strain is very small, due to the near-cancellation of the two sources, and is estimated to be less than one nanostrain, and the corresponding displacement of the order of micrometres. Given that the time constant for this change is probably a few months, such an event is undetectable, geodetically.

22. Snieder, R., Grêt, A., Douma, H. & Scales, J. Coda wave interferometry for estimating nonlinear behavior in seismic velocity. *Science* **295**, 2253–2255 (2002).
23. Okada, Y. Internal deformation due to shear and tensile faults in a half-space. *Bull. Seismol. Soc. Am.* **82**, 1018–1040 (1992).

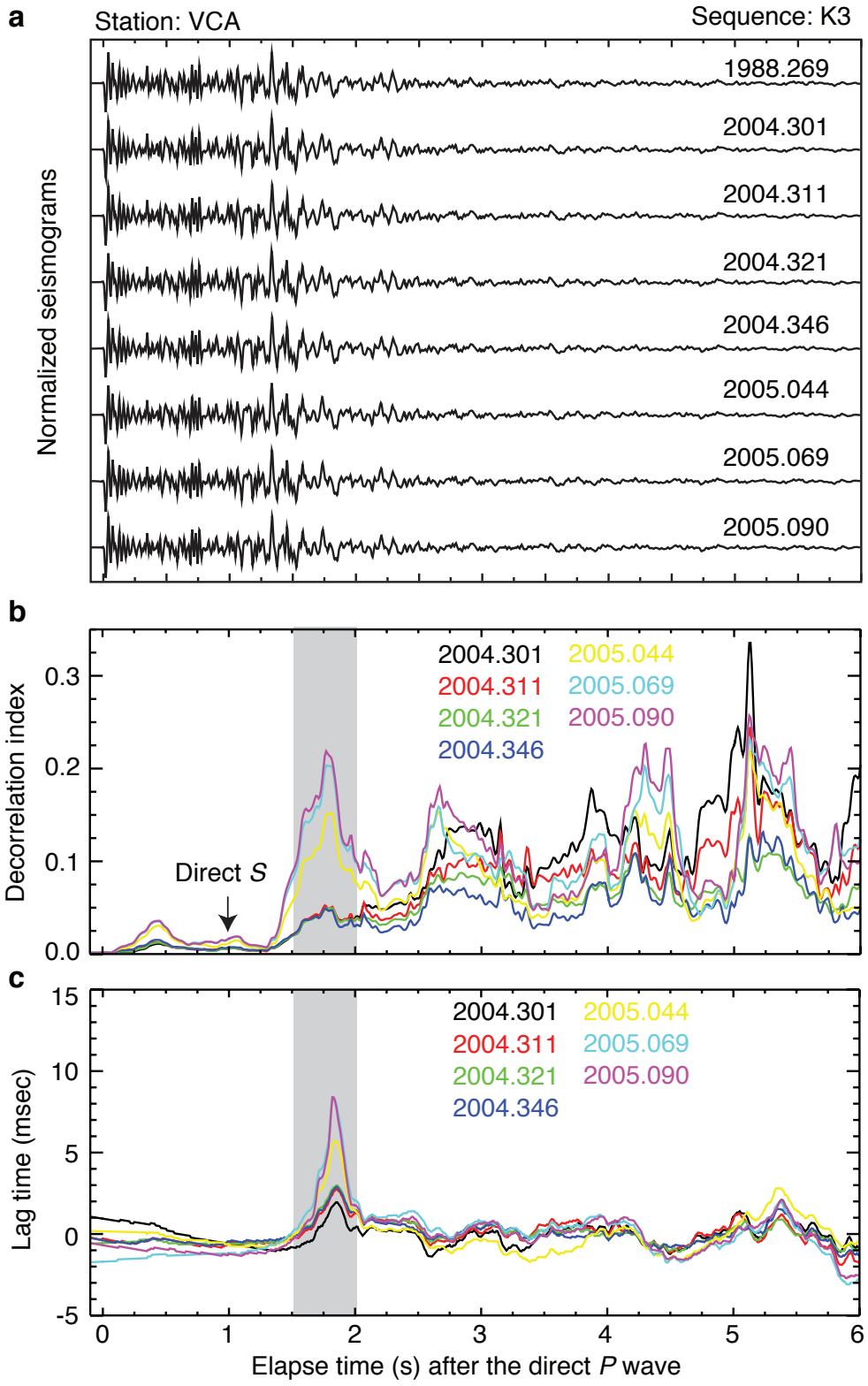

Supplementary Figure 1: Example changes in waveforms associated with temporary changes in the scatterer properties of the target scatterer and their decorrelation index and lag time. **a,** Observed vertical seismograms at station VCA for 8 repeating earthquakes in sequence K3. Calculated decorrelation index $D(t)$ (**b**) and lag time $\tau(t)$ (**c**). A linear trend in lag time, most likely due to shallow velocity

reduction induced by the local 2004 Parkfield earthquake[24], is removed. All waveforms are aligned to the direct *P* wave. Note that remarkable increases in both $D(t)$ and $\tau(t)$ at 1.8 s between the 11 December 2004 earthquake (blue) and the 13 February 2005 earthquake (yellow). The 1.8-s elapsed time of isolated spikes in $D(t)$ and $\tau(t)$ would correspond to temporal variations in scatterer properties of the target scatterer, given the same elapsed time in ref. 4.

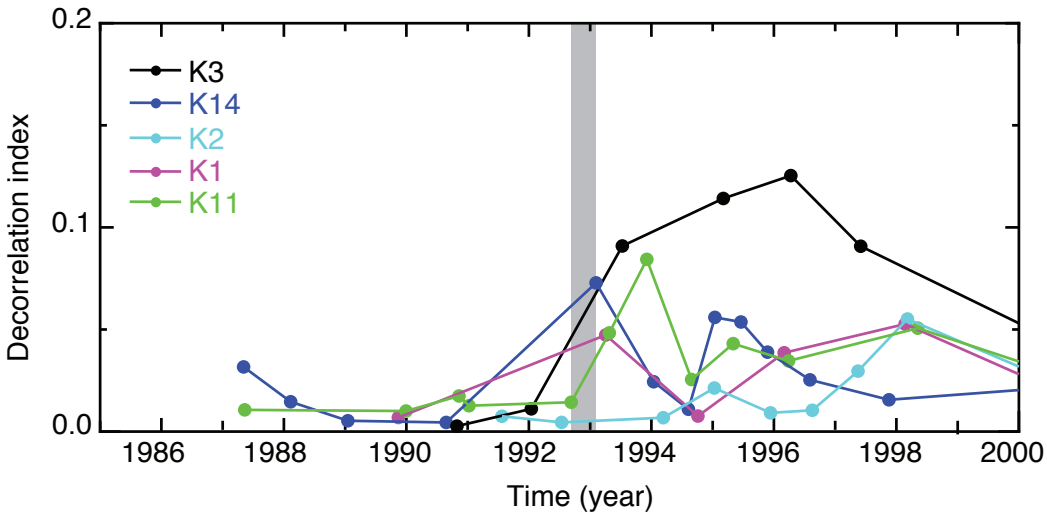

Supplementary Figure 2: Initiation of the 1st excursion in the target scatterer properties. Decorrelation index, $D(t)$ for the station VCA that is one of lowest-noise stations (see Methods) reflecting scatterer properties of the target scatterer for sequences K3, K14, K1, K2 and K11. The first 4 sequences were used to examine temporal evolution in $D(t)$, and the onset time of the 1st excursion in $D(t)$ was constrained to be within the 7 month period of 14 July 1992 (sequence K2) and 5 February 1993 (sequence K14) (ref. 4). We found that sequence K11 provides an additional constraint of the onset time, reducing the interval to the 5-month period between September 10, 1992 and February 5, 1993.

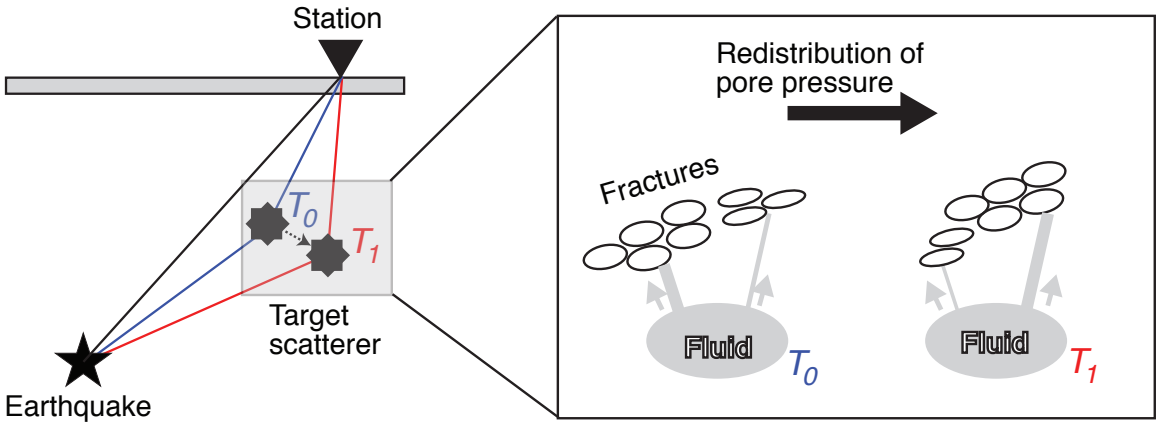

Supplementary Figure 3: A schematic view of temporal change in the target scatterer. On the left, the change in seismic ray-path due to a change in scatterer properties. On the right, change in the fracture (i.e., scatterer) geometry is the result of stress-induced fluid redistribution, which also produces a corresponding redistribution of pore pressure. Such a change in fracture geometry will lead to temporal changes in the seismic raypath illustrated in the left side. In addition, the pore pressure change can alter the strength of the fault through its influence on the effective normal stress.

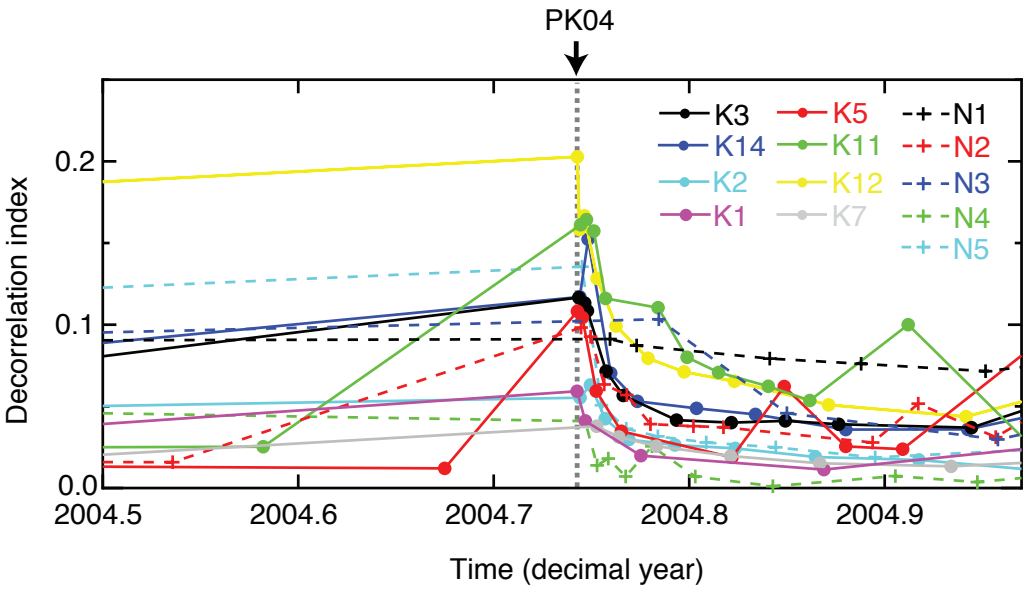

Supplementary Figure 4: Initiation of the 2nd excursion in target scatterer properties. Same as Fig. S2 for all available repeating-earthquake sequences that we have examined, for a 6-month time period including the occurrence of the 2004 Parkfield earthquake (PK04).

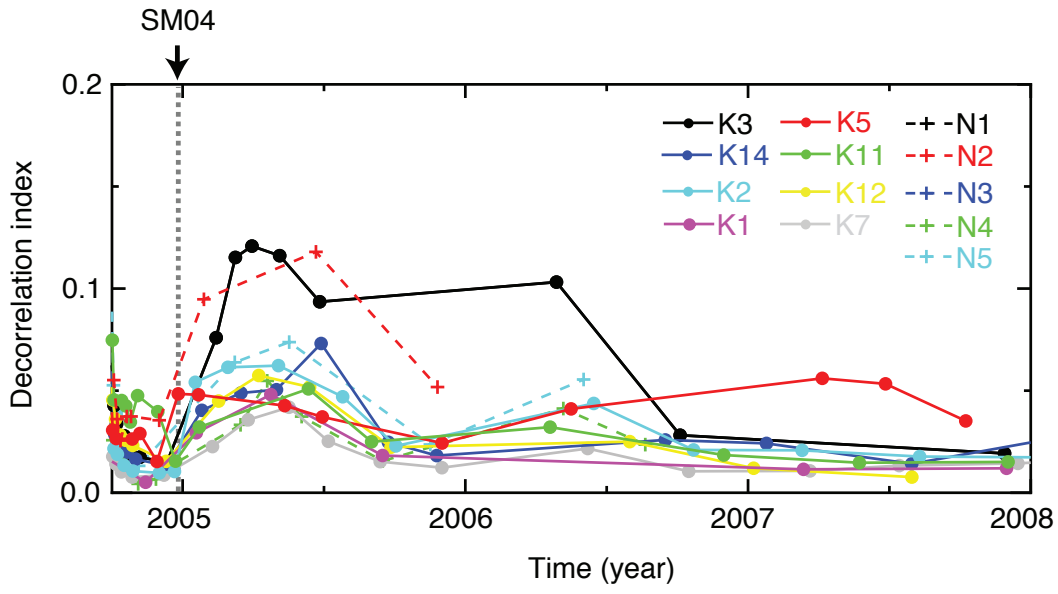

Supplementary Figure 5: Duration of the 3rd excursion in the target scatterer properties. Average $D(t)$ is shown for late 2004 to 2008 time period using the three lowest-noise stations: VCA, LCCB and CCRB. Note that excursion has duration of about one year. Average $D(t)$ was plotted if individual $D(t)$ for all those three stations are available.

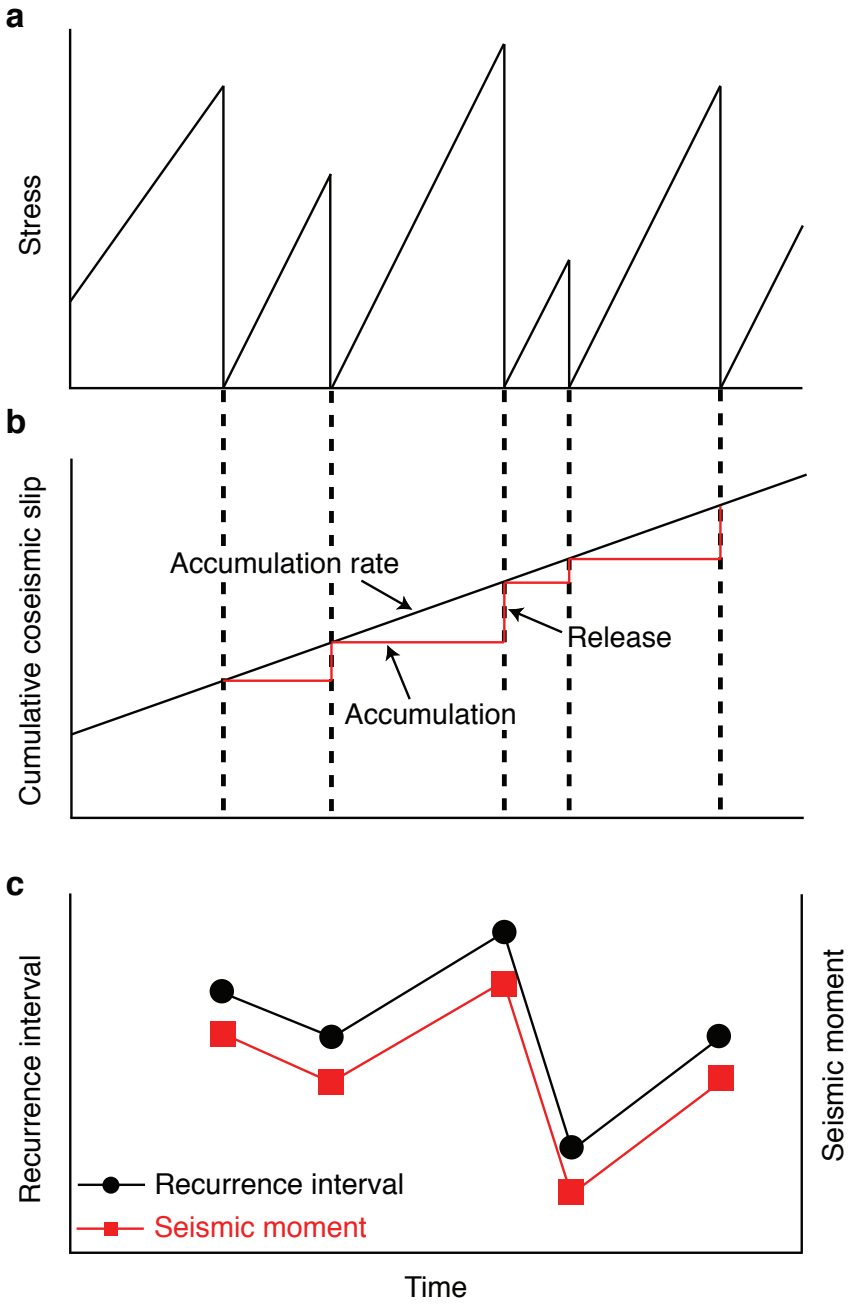

Supplementary Figure 6: A schematic view of slip-predictable model. Time histories of loading stress (**a**), cumulative coseismic slip (**b**) and expected recurrence interval and seismic moment (**c**) for slip predictable model[16]. This assumes that rupture area is constant and stress drop is complete, so that slip, and hence M_0 is proportional to stress drop. In this case, for constant loading rate, M_0 and T_r covary, and are both proportional to fault strength. A weakened fault produces both a shorter recurrence interval and lower stress drop and *vice versa*.

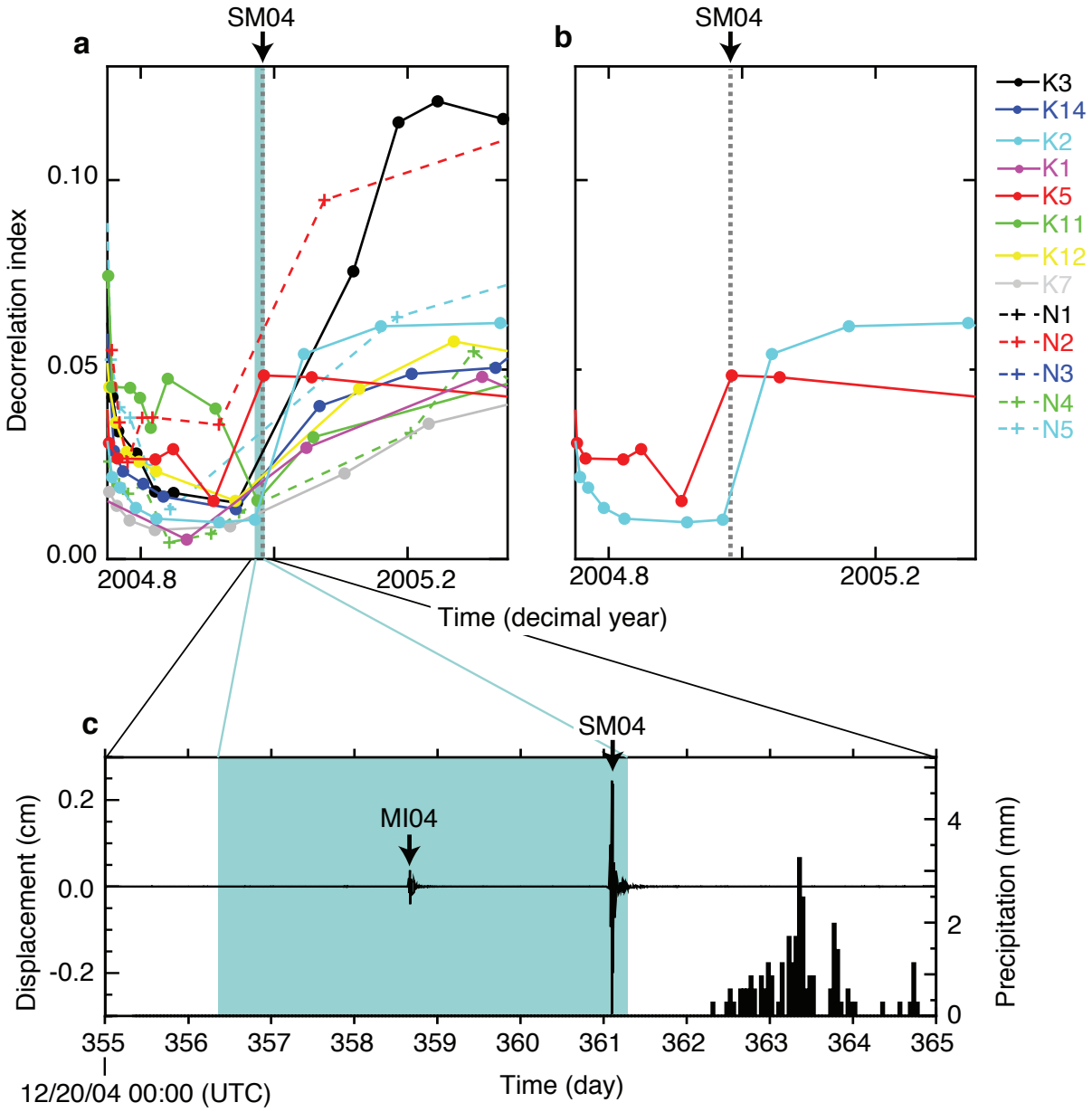

Supplementary Figure 7: Initiation of the 3rd excursion in the target scatterer properties. a, Same as Fig. S5, for a 6-month time period close to the occurrence of the 2004 Sumatra-Andaman earthquake (SM04). **b**, Same as (**a**) but only showing $D(t)$ for sequences K2 (light blue) and K5 (red). For both sequences, the estimated noise levels are less than the size of the excursion. Those sequences constrain the onset interval to be a ~5-day time period (21-26 December, 2004). The initiation of the 3rd excursion in $D(t)$ is seen to occur in an interval that includes the 2004 Sumatra-Andaman earthquake (SM04) which occurred 7 hours before the end of the interval. **c**, Band-pass filtered (0.01-0.1 Hz) vertical broadband seismogram recorded at the Parkfield area, during 20-30 December 2004. Also shown is 1-hour-sampled precipitation data at this area. MI04 denotes the 23 December 2004 M_w 8.1 North of Macquarie Island earthquake. The maximum dynamic stress change (proportional to

displacement) for the 2004 Sumatra-Andaman earthquake is nearly an order of magnitude greater than one for the 2004 North of Macquarie Island earthquake. The change in fault strength we observe is most likely due to a redistribution of pore pressure caused by the dynamic stresses produced by the 2004 Sumatra-Andaman earthquake.

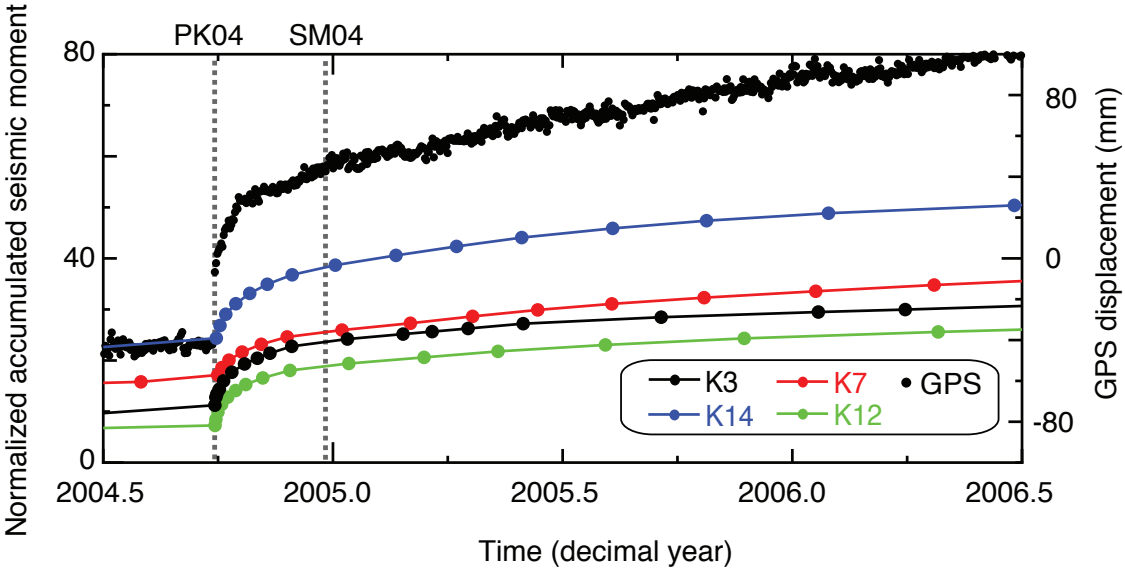

Supplementary Figure 8: Accumulated seismic moment (colored circles) from repeating-earthquake sequences with GPS displacement (black dots) in the pre- and post-Parkfield earthquake periods. We used 1-day solutions of west-east GPS displacement recorded at Pomm, Parkfield, determined by U.S. Geological Survey (http://quake.wr.usgs.gov/research/deformation/gps/auto/ParkfieldContin/pomm/index .html). There are no abrupt changes in either accumulated seismic moment or GPS displacement associated with the 3rd excursion in decorrelation index that we found around the time of the 2004 Sumatra-Andaman earthquake. Vertical dashed-gray lines are the occurrence times of the 2004 Parkfield earthquake (PK04) and the 2004 Sumatra-Andaman earthquake (SM04).

Supplementary References

24. Rubinstein, J. L. & G. C. Beroza, G. C. Depth constraints on nonlinear strong ground motion from the 2004 Parkfield earthquake. *Geophys*. *Res*. *Lett*. **32**, L14313, doi:10.1029/2005GL023189 (2005).